Acta Oceanol. Sin., 2021, Vol. 40, No. 1, P. 103–112
https://doi.org/10.1007/s13131-020-1672-3
http://www.hyxb.org.cn
E-mail: hyxbe@263.net

Response of the upper ocean to tropical cyclone in the Northwest Pacific observed by gliders during fall 2018

Zekai Ni[1, 2], Jiancheng Yu[3], Xuekun Shang[1], Wenming Jin[3], Yeteng Luo[3], Philip A Vetter[1], Huichang Jiang[1], Liu Yu[1], Sumin Liu[1], Hongzhou Xu[1]*

[1] Institute of Deep-sea Science and Engineering, Chinese Academy of Sciences, Sanya 572000, China

[2] Graduate School, University of Chinese Academy of Sciences, Beijing 100049, China

[3] Shenyang Institute of Automation, Chinese Academy of Sciences, Shenyang 110169, China

Received 8 June 2020; accepted 15 June 2020

Abstract

The evolution of thermohaline structure at the upper ocean during three tropical cyclones (TCs) in the Northwest Pacific was studied in this study based on successive observation by two new-style underwater gliders during fall 2018. These remote-controllable gliders with CTD sensor enabled us to explore high frequency responses of temperature, salinity, mixed and barrier layers in the upper ocean to severe TCs in this area. Results showed that three significant cooling-to-warming and stratification destructing-to-reconstructing processes at the mixed layer occurred during the lives of three TCs. The maximal cooling of SST all reached $\geqslant$0.5°C although TCs with different intensities had different minimal distances to the observed area. Under potential impacts of solar radiation, tide and inertial motions, the mixed layer depth possessed significant high-frequency fluctuations during TC periods. In addition, barrier layers appeared and vanished quickly during TCs, accompanied with varied temperature inversion processes.

Key words: mixed layer depth, barrier layer, tropical cyclone, underwater glider, Northwest Pacific

Citation: Ni Zekai, Yu Jiancheng, Shang Xuekun, Jin Wenming, Luo Yeteng, Vetter Philip A, Jiang Huichang, Yu Liu, Liu Sumin, Xu Hongzhou. 2021. Response of the upper ocean to tropical cyclone in the Northwest Pacific observed by gliders during fall 2018. Acta Oceanologica Sinica, 40(1): 103–112, doi: 10.1007/s13131-020-1672-3

1 Introduction

Tropical cyclone (TC) is a severe atmospheric event nourished by the upper ocean through air-sea interaction (Price, 1981; Emanuel, 1986). In return, the upper ocean is modulated by TCs both in thermodynamics and hydrodynamics, which may even have an impact on large-scale ocean circulation and the climate system (Emanuel, 2003; Sriver and Huber, 2007; Dare and McBride, 2011; Hart, 2011). Every year, an average of about 86 TCs occur in tropical regions around the world. Among several sources of TCs, the Northwest Pacific (NWP) is the most active area, accounting for around one-third of all TCs worldwide (Elsner and Liu, 2003; Guo and Tan, 2018). On the other hand, understanding of the upper ocean response to TCs is important for accurate TC prediction. Yet few researches have studied the upper ocean response to TCs in the NWP based on detailed and integrated observation. There is still uncertainty in many processes because of the lack of *in-situ* observation.

The cooling of the sea surface temperature (SST) is the most significant consequence caused by TC (Emanuel, 2003; Wang et al., 2016). The maxima of SST reduction by TCs can range from less than 1°C up to 9°C (Cione and Uhlhorn, 2003; Lin et al., 2003; Walker et al., 2005; Meyers et al., 2016; Zhang et al., 2018). It takes a few days to weeks for SST to restore in the wake area (Emanuel, 2001; Dare and McBride, 2011; Hart, 2011; Vincent et al., 2012b). The SST cooling by TC is primarily due to three main processes: enhanced latent and sensible heat fluxes from the water to the air, entrainment mixing of cold water at the mixed layer base induced by heavy wind shear instability, and upwelling induced by wind curl. Among them, entrainment mixing and upwelling are considered to be the dominant processes for cooling under fast- and slow-moving TCs, respectively (Huang et al., 2009; Price, 1981). The air-sea heat flux is unignorable for the case of weak TC (Vincent et al., 2012a).

Furthermore, TCs change the depth and structure of mixed layer of the upper ocean. It is generally recognized that a powerful tropical cyclones can deepen mixed layer depth (MLD) (Bender et al., 1993; Ginis, 2002; Pan and Sun, 2013). Liu et al. (2007) found more complex results of both deepening and shoaling of TC impact on the MLD by comparison of pre- and post-storm Argo profiles, and attributed the deepening to vertical entrainment mixing and the shoaling to upwelling of thermocline. Yang et al. (2015) reported that enhanced vertical mixing can lead to destruction of the stratification of mixed layer during TC period.

Moreover, TCs influence the variation of barrier layer. Acting as a "barrier" in heat exchanging and turbulent mixing between

Foundation item: The National Key R&D Program of China under contract No. 2018YFC0309800; the National Natural Science Foundation of China under contract Nos 41666001, 41576006, 41676015 and U1709202; the Strategic Priority Research Program of the Chinese Academy of Sciences under contract No. XDA13030302; the Chinese Academy of Sciences Frontier Basic Research Project under contract No. QYJC201910.

*Corresponding author, E-mail: hzxu@idsse.ac.cn

mixed layer and thermocline, the presence of barrier layer affects the mixed layer variation under TC conditions (Sprintall and Tomczak, 1992; Balaguru et al., 2012; Domingues et al., 2015). A pre-existing barrier layer is able to mitigate the SST-cooling response by as much as 0.4–0.8°C/d (Wang et al., 2011). Zhang et al. (2019) reported that TCs can either intensify or weaken a pre-existing barrier layer through processes of vertical mixing, upwelling and precipitation, and it even can build a new one or destruct a pre-existing one in some cases.

There are many ways for scientists to observe the upper ocean changes caused by TC. With the development of satellite technology, it is convenient to get high-spatial-resolution data like air pressure, SST, surface wind field, and precipitation. However, satellite observations are constrained to the sea surface and low temporal resolution of more than 1 d. Shipborne CTD instrument provides a good chance to observe oceanic thermohaline fine structure, but it is limited by the harsh weather conditions during TC. Mooring buoy is unaffected by severe weather usually, but it carries too few instruments to measure detailed vertical thermohaline structure in vertical in the upper ocean. Argo floats provide high quality real-time profile data of temperature and salinity. However, their temporal resolution with more than 6 d interval is very low and they are unable to be guided to the targeted region by remote control. To extract the TC-induced variation signal from the Argo floats dataset, a very large number of pairs of pre- and post-storm profiles usually were necessary (Jourdain et al., 2013; Wu and Ling, 2015; Steffen and Bourassa, 2018).

Underwater gliders with CTD sensors are a new type of instrument effective at measuring the upper ocean physical structure even in severe oceanic conditions. It can work persistently for several months under control by scientists on land. Moreover, it has the ability of collecting datasets with higher vertical resolution and sampling frequency compared to Argo floats. By using this type of instrument, Domingues et al. (2015) analyzed the upper ocean response to TC-induced winds in South Puerto Rico of Caribbean Sea. In recent years, the Chinese Sea-wing underwater glider has been applied to many oceanic researches and observations, such as sea surface cooling (Qiu et al., 2015), mesoscale eddies (Shu et al., 2016; Qiu et al., 2019b, 2009c) and assimilation (Peng et al., 2019).

In the fall of 2018, two new type of Chinese Sea-wing 7 000-m gliders with CTD-37 sensor were deployed to collect hydrologic data at the "Challenger Deep" of the Northwestern Pacific during the cruise of R/V *Tansuoyihao*. During the period, three TCs named Mangkhut, Trami and Kong-Rey passed nearby the area and the gliders captured the variation of the local upper ocean response to the TCs. Based on the thermohaline profile dataset collected by the two gliders, we described the local upper ocean response to the three TCs, including surface cooling, destratification of mixed layer, and the emergence and disappearance of barrier layer. Then, we discussed the possible physical mechanism behind them.

2 Data and methods

We used reanalysis product ERA5 from the European Centre for Medium-Range Weather Forecasts (ECMWF) to illustrate meteorological conditions during the TCs. Assimilating multi-resource observation data with physical model, the ERA5 dataset provides data including SST, 10-m wind, surface latent and sensible heat flux, precipitation rate, and evaporation of ocean surface with a spatial-resolution of 0.125°×0.125° and a temporal resolution of 1 h. Track data of the TCs were obtained from the National Meteorological Center of China Meteorological Administration (http://typhoon.nmc.cn/) and the Regional Specialized Meteorological Center of Japan Meteorological Agency (http://www.jma.go.jp/jma/index.html). The former has more specific classification of intensity level of TCs and higher temporal frequency, while the latter contains preliminary data taken before a TC is formally declared. Therefore, the two datasets were combined to show the precise tracks of the TCs (Fig. 1a).

The first glider (Glider 1) deployment covered the period from September 9 to October 5 and performed 52 pairs of descending and ascending profiles in 27 d. Another glider (Glider 2) was deployed on September 15 and recovered the same day as the first one. It performed 50 pairs of descending and ascending profiles in 21 d (Fig. 1b). In this study, the ascending data from 300 m depth to surface were interpolated with 1 m interval. The observed region was about 140 km×85 km. To check the consistency between two gliders, we averaged the profile dataset for each one from September 15 to October 5 and plotted in Fig. 2. It can be seen that there was high concordance between the two averaged profiles in the upper mixed layer and deeper layer.

There is a wide range of defining methods for the MLD which vary with different areas and research themes, including threshold criteria, gradient criteria, buoyancy frequency criteria, and so on (Thomson and Fine, 2003; Holte and Talley, 2009; Carvalho et al., 2017; Steffen and Bouras, 2018; Qiu et al., 2019a). In this study, we used the MLD defining method based on buoyancy frequency (N) rather than traditional threshold or gradient criteria methods. The buoyancy frequency was calculated as:

$$N^2(z) = -\frac{g}{\rho}\frac{\mathrm{d}\rho}{\mathrm{d}z}. \tag{1}$$

The method performed better when stratification changes largely in the upper ocean (Carvalho et al., 2017). Buoyancy frequency usually reach peak at bottom of stratified layer. The depth with the first significant peak of the N was regarded as the thickness of the mixed layer. In the case of existence of a barrier layer, its thickness was calculated as the depth difference between two remarkable peaks.

3 Results

3.1 *TC Mangkhut event*

TC Mangkhut was originated from a tropical depression near the Bikini Atoll on September 6, 2018. It was developed to a typhoon (12th grade) on September 9 and upgraded to a severe typhoon (15th grade) when it was closest to the observed region on September 11, with a mean 7th grade wind radius of 275 km. Then, it left the region on September 12 as a 18th grade super typhoon (Fig. 1a). Figure 3 shows the observed region was occupied by a warm core with highest temperature around 30°C before approach of TC Mangkhut on September 10. A day later, the warm core was eliminated and replaced by a cold wake due to approach of the TC. This cold wake lasted more than ten days till the next TC. Both gliders and satellite SST data showed the decrease of mixed layer temperature reached about 0.7°C during TC Mangkhut (Fig. 4a). The temperature began to restore on September 14. Correspondingly, wind speed and evaporation began to increase on September 10, and the net heat flux became toward air from ocean surface which led to decreasing the mixed layer temperature. The wind speed and evaporation rate reached the maximum values on September 11 as TC Mangkhut made it closest to the observed region (Figs 4c and d). At the same day, the loss of heat content reached the maximum value accompan-

ied by the largest drop of air pressure. The precipitation rate rose to a relatively high level on September 11 and lasted for three days. However, salinity at the mixed layer observed by gliders showed increasing trend possibly due to its spatial nonuniformity of precipitation during the period.

The fast-growing wind stirred and deepened mixing layer gradually through change of salinity, temperature and density structures since September 9, eventually leading to the destruction of the mixed layer stratification (Fig. 5f). And the MLD was deepened to lower than 60 m depth at the beginning of September 10 (Fig. 5d). However, the mixed layer was elevated about 20 m after six hours indicating a large vertical fluctuation of the MLD induced by internal tide or near inertial oscillations (Fig. 5e). Another six hours later, the MLD was deepened again to below 60 m (Fig. 5f). TC Mangkhut left the observed region at September 11 resulting in a warmer and shallower MLD with a thickness of 25 m (Fig. 5g). Eventually, the MLD kept a stable value of about 47 m after the whole process (Figs 5h–l).

3.2 *TC Trami event*

TC Trami was originated from a tropical depression on the east 530 km from the observed region on September 20 (Fig. 1a).

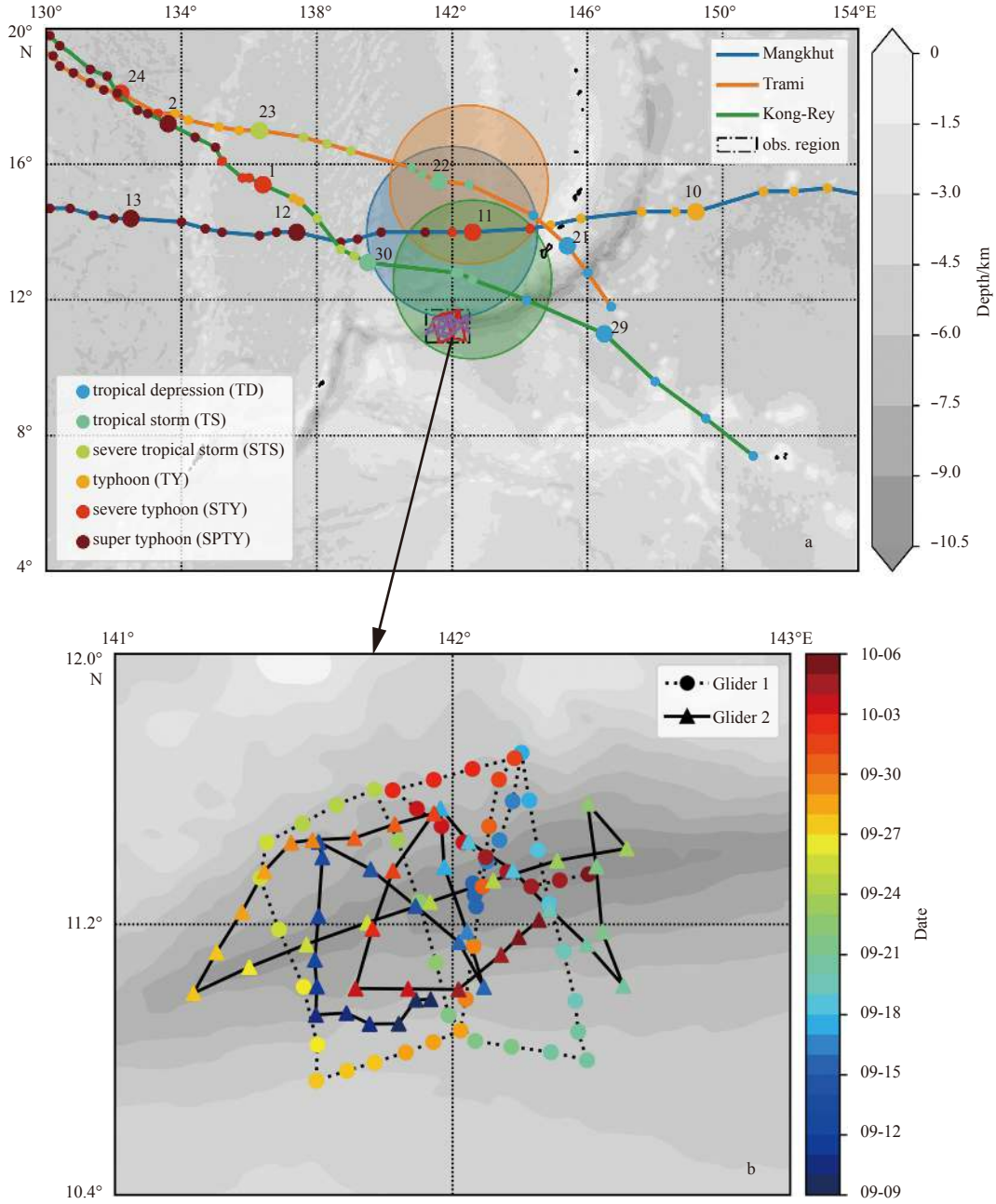

Fig. 1. The tracks of three TCs (a) and glider pathway during the cruise (b). In a, the colored dots illustrate the location and intensity level of TC, larger dots indicate every first point of a day and text above shows the date; rough ranges of 7th grade wind of each TCs when they are closest to the observed region are illustrated as translucent circles (only for TC level over TS); grey background indicates the topography. In b, the paths of Glider 1 and Glider 2 are marked with dotted and solid lines, respectively; profile locations are marked with circular or triangular markers whose color indicates the observation date.

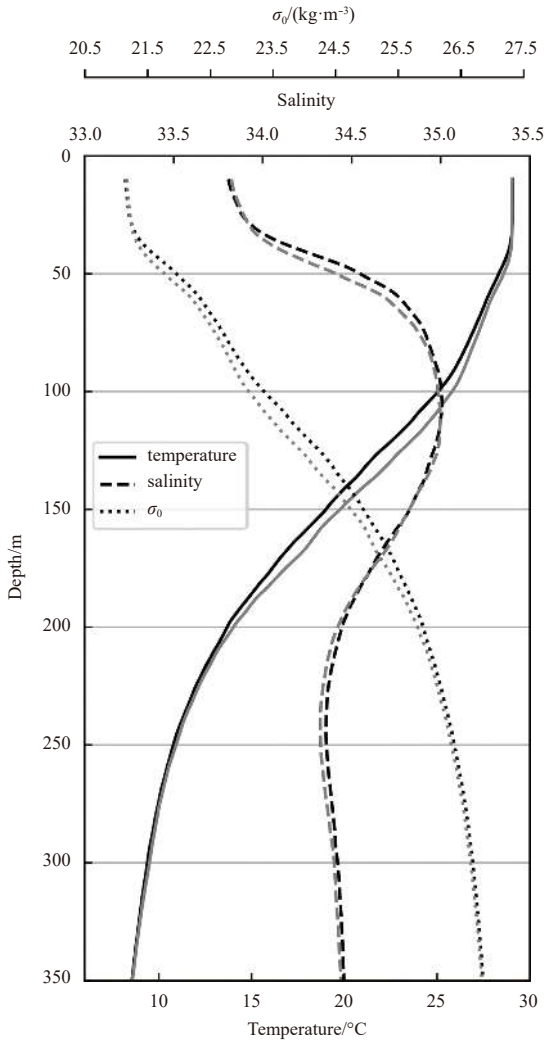

Fig. 2. Comparisons of averaged thermohalinic profiles from two gliders for the same period from September 15 to October 5. Variable σ_0 is the potential density anomaly with respect to 1 000 kg/m^3. Black and grey lines represent Glider 1 and Glider 2, respectively.

It moved northwestwards and strengthened to a tropical storm (8th grade) on September 21 at 16:00, with a mean 7th grade wind radius of 255 km. During the period, it reached the minimum distance from the observed region on September 21 at 10:00. After the period, TC Trami was strengthened to severe typhoon (14th grade to 17th grade) on the way heading northwestwards.

TC Trami also generated a cooling effect at the surface as the former one and led to similar cold wake (Figs 3e and f). The glider results showed that the temperature at the mixed layer was decreased gradually since the tropical depression formed and it ended up on September 25 with total drop of 0.5°C (Fig. 4a). Once TC Trami developed to a typhoon, the regional wind speed reached the maximum value on September 23, as did the evaporation rate, latent heat flux, net heat flux and precipitation rate (Fig. 4).

Compared with TC Mangkhut, TC Trami was much weaker and farther from the observed region although it yielded the similar maximum wind speed. And it has relative weak impact on the upper ocean thermohaline structure compared with the former one (Figs 5 and 6). The deepening of the mixed layer was about 10 m and the MLD reached about 50 m which was less than the prior results. As intensified TC Trami approached the observed region, the mixed layer boundary became hard to identify because of the weakness of vertical stratification, and more heat was taken to the sub-surface layer (Figs 6f and m). It can be seen that the temperature profiles from the mixed layer bottom to the thermocline varied more gently compared to that during pre-TC. Consequently, the stratification was weakened much slighter than before. A barrier layer was shown up on September 22 in a profile of Glider 1, but none can be seen from the profile of Glider 2 at the same time (Figs 6g and n). We assumed the barrier layer was generated by the advection mechanism, in which the wind-driven current brought water mass with high temperature and low salinity to the mixed layer at the certain area, and local cold water subducted and replaced by warm water at the mixed layer that generate a clear two layer stratification in the upper ocean. The barrier layer was short-lived and can easily be destroyed by strong wind (Figs 6h–j). Another barrier layer was detected by Glider 2 and there was a low temperature and salinity water mass formed above the barrier layer on September 24 and 25 (Figs 6r–t). Given the absence of strong precipitation, this layer may have been caused by the advection from other area with heavy precipitation and its stratification was too weak to claim a new mixed layer.

3.3 *TC Kong-Rey event*

TC Kong-Rey was formed from a tropical depression at the southeast of the observed region on September 28 and moved northwestward (Fig. 1a). Compared to the previous two TCs, its pathway was the closest to the observed region. The distance between the region and the TC track reached a minimum of 170 km on September 29 at 16:00, while the TC was a tropical storm (8th grade) with a mean 7th grade wind radius of 255 km. The temperature profiles from two gliders showed that the drop of the mixed layer temperature started on September 28 18:00 when Kong-Rey was about 700 km away from the observed region and ended on October 1 (Fig. 4a), with total drop of around 0.7°C. However, the decrease of temperature was insignificant based on the satellite-observed SST dataset. Figure 4f shows that solar radiation has low values from September 29 to October 4 indicating that the high rate of cloud cover might have blinded the satellite and led to inaccurate observation of SST.

Due to the proximity between TC center and the observed region, TC Kong-Rey brought abundant rainfall to this area and led to a sharp decline of mixed layer salinity (Fig. 4). As a result, massive freshwater was injected into the local ocean surface that led to the formation of the barrier layer. The ILD also was regarded as an indicator for defining the mixing depth. Based on that, the vertical mixing can reach about 60 m depth on September 28 (Fig. 7c). Figure 7c shows a thick barrier layer about 45 m was generated due to the heavy precipitation on September 28 13:00 based on Glider 1's observation. With deepening of the isopycnic layer, the barrier layer thickness was reduced to 15 m at 21:00, and temperature inversion was generated. At September 29 4:00, the barrier layer disappeared, and the temperature inversion was nearly erased. After that, the barrier layer and inverse-thermal layer occurred again as shown due to more heavy rainfall on September 29 17:00 (Fig. 4i). the barrier layer eventually disappeared in the night. Observation from Glider 2 shows a different development. In profiles shown in Figs 7o and f (one hour and 62 km apart), an inverse-thermal barrier layer was also detected. However, Fig. 7o has not shown a sub-halocline structure within the barrier layer compared to Fig. 7f. It is more like the profile in Fig. 6r, in that they were mostly caused by surface

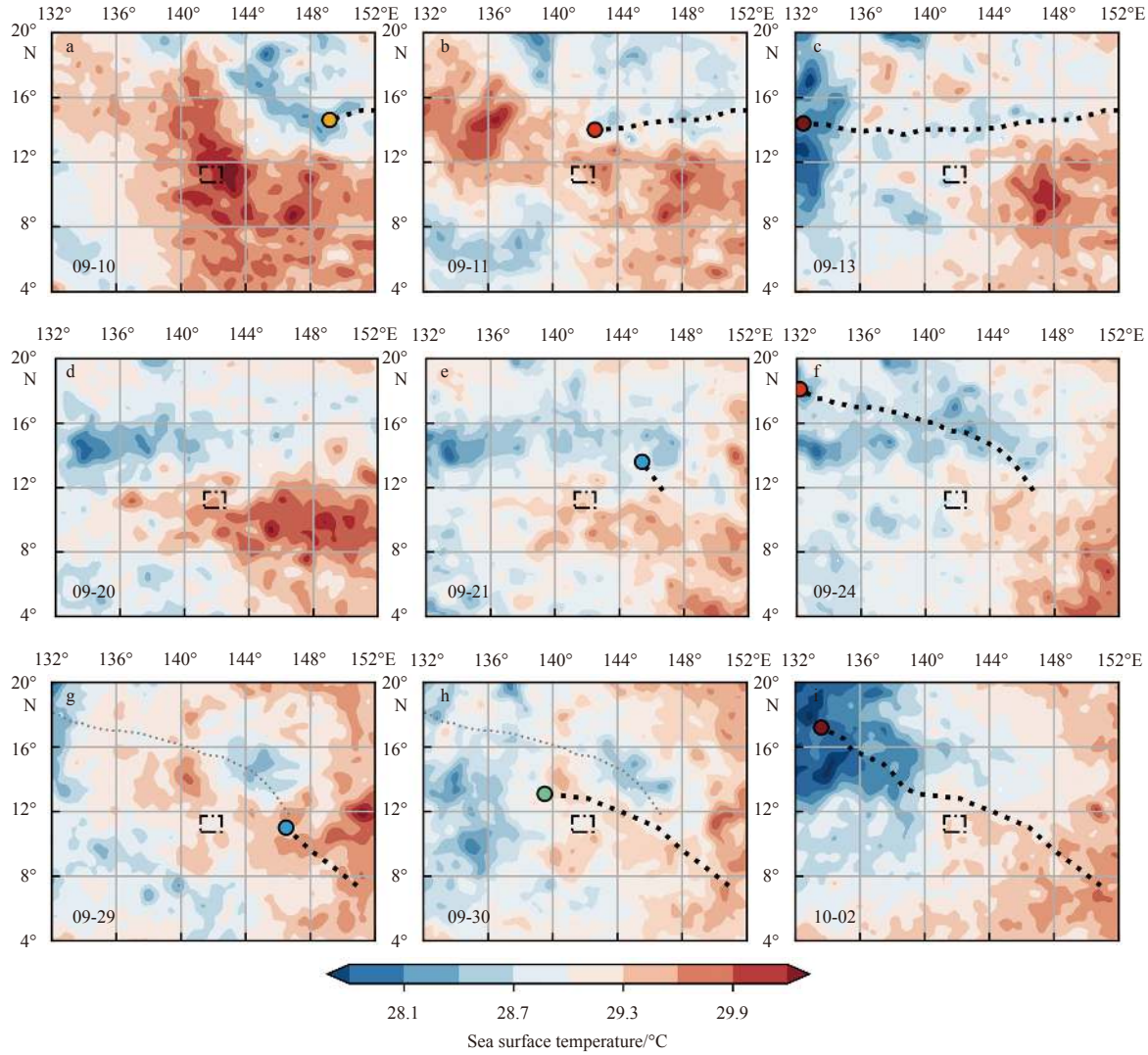

Fig. 3. Satellite-observed sea surface temperature demonstrated by background color during the period. The tracks of TCs are shown as dotted lines with colored circles representing the intensity level (reference the color table in Fig. 1). The dates are shown in lower left corner of every graph.

advection from the low salinity area which had been recently rained upon.

4 Discussion

4.1 *SST cooling*

The cooling-warming processes of SST response to the three TCs were clearly depicted based on our *in-situ* glider observation. However, compared to previous reports about TC-induced cooling event, the cooling processes in this study were relatively moderate. The maximum SST drops were 0.7°C, 0.5°C and 0.7°C, respectively, due to long distances between the observation region and TC's centers with values of 315 km, 455 km and 172 km. Note that for all three TCs, our observation region was located on the left side of the storm tracks which might weaken the cooling effects; in the northern hemisphere, SST cooling is typically greater on the right side (Lin et al., 2003; D'Asaro et al., 2007; Zhang et al., 2016). Yang et al. (2015) reported that the maximum SST cooling can reach about 1.5°C (4.4°C) at the region with 120 (50) km distances right of the tropical storm Washi (typhoon Damrey) based on buoy data during 2005. Even more, Zhang et al. (2016) showed that the maximum cooling can reach about 2.5°C at the region with 144 km distance right to Typhoon Kalmaegi during 2014.

Generally, stronger TC can cause stronger SST cooling. And the farther away, the smaller the impact of SST. However, the three TCs with different intensities and distances with observed region caused almost the same SST cooling $\geqslant$0.5°C. We assumed that it might be related to their fast translating speed (i.e., around 6.7 m/s, 8.3 m/s, and 6.4 m/s, respectively) compared to others. Mei et al. (2015) stated that the SST cooling by weak and fast TCs with translation speed $\geqslant$3 m/s and intensity $\leqslant$33 m/s was around 0.5°C within 3°×3° area of TC trails in the Northwest Pacific.

Our results showed that there was SST bias existed between glider observation and ERA5 dataset during TCs. The SST from ERA5 only showed cooling processes during the first two TCs. no SST drop was found during TC Kong-Rey and the SST restorations after TCs Trami and Kong-Rey were insignificant (Fig. 4a, SST). The ERA5 dataset has assimilated several satellite-observed SST data based on thermal infrared and microwave remote sensors, which may lead to large error by clouds, aerosols or

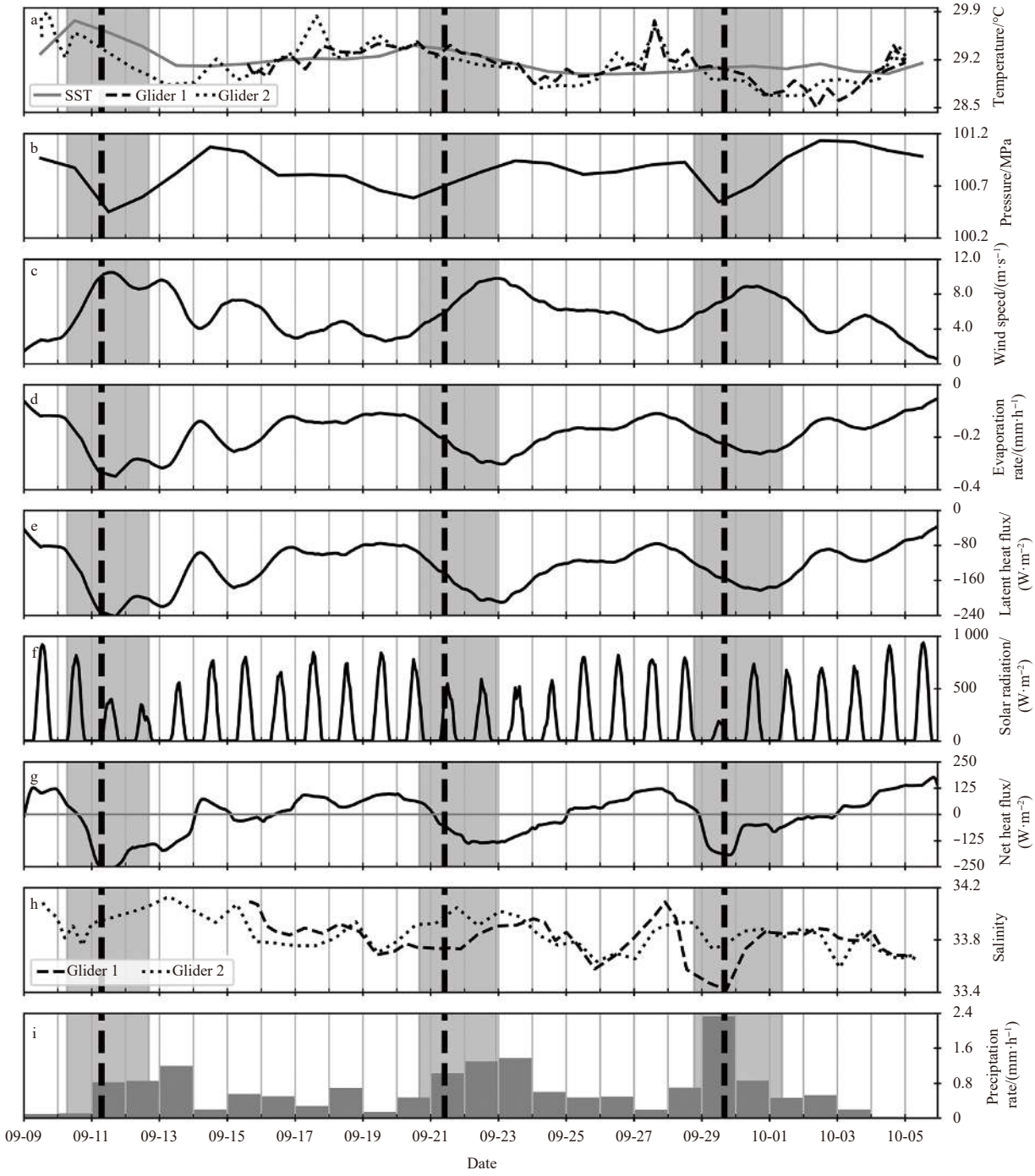

Fig. 4. Variables curves are from ERA5 or glider observation. For evaporation rate and latent heat flux, negative phases mean the direction is from ocean surface to the air. Shaded areas indicate when a TC was within 700 km of the observed region, and bold-dotted lines indicate the time when a TC is nearest.

water vapor during severe weather conditions (Liu et al., 2014). Previous studies revealed that the difference between satellite-derived SST and oceanic surface temperature from *in-situ* measurements mostly ranged from 0.3°C to 0.7°C (Bhaskar et al., 2009; Kim et al., 2010). Hence, satellite observation may be unable to capture the small change of the SST response to TCs.

4.2 *Mixed layer fluctuation*

It has been known that TC-induced strong wind stress enhances turbulent and entrainment mixing of the upper ocean that leads to the deepening of mixed layer (Bender et al., 1993; Ginis, 2002; Pan and Sun, 2013). However, other processes also can influence the variation of MLD. For example, vorticity and convergence input from the TC have been found to cause upwelling of deeper water and decrease the MLD in the South China Sea (Zhang et al., 2016). In addition, diurnal internal tides can outweigh TC-induced near-inertial oscillations in some cases reported by Yang et al. (2015). Moreover, even solar radiation can lead to diurnal variation of MLD (Sutherland et al., 2014). Compared to pre- and post-TC profiles (Figs 5d and f), the

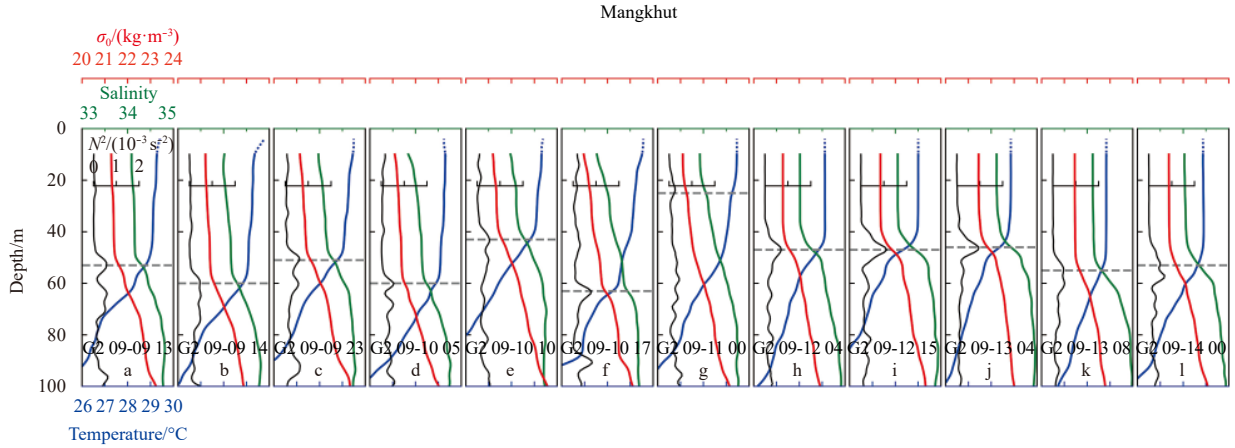

Fig. 5. Sequence of thermohalinic profiles during TC Mangkhut. Texts inside frame identify the gliders (G1 for Glider 1, G2 for Glider 2), dates and hours. Horizontal dotted lines indicate the MLD (in grey) or ILD (in blue, in case not equal to MLD).

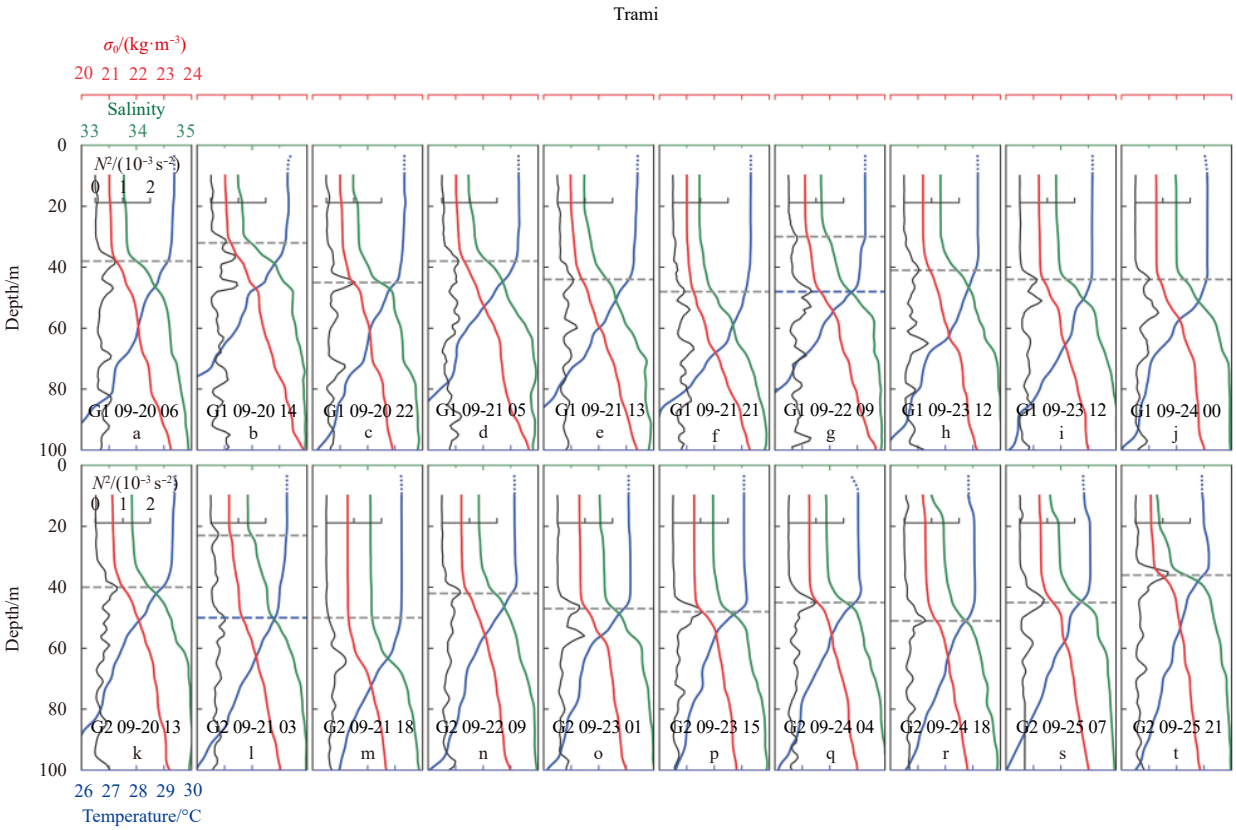

Fig. 6. Sequences of thermohalinic profiles during TC Trami. Texts inside frame identify the gliders (G1 for Glider 1, G2 for Glider 2), dates and hours. Horizontal dotted lines indicate the MLD (in grey) or ILD (in blue, in case not equal to MLD).

profile in Fig. 5e shows an evident uplift of mixed layer, which might be due to internal tide or near-inertial oscillations in this area. Several similar fluctuations on MLD also were found in Figs 6 and 7. To explore the detail, high-frequency observation of thermohaline structures will be required.

4.3 *Barrier layer formation*

As described in Sections 3.2 and 3.3, several barrier layers showed up during TCs Trami and Kong-Rey and vanished very quickly in this study (Figs 6 and 7). However, Wang et al. (2011) found that pre-existing barrier layers persisted throughout the whole period of TC. The formation mechanisms of barrier layer can be generally classified into two broad types: local surface freshening (e.g., rainfall), and subduction and advection processes (Cronin and McPhaden, 2002). TC-induced barrier layer mostly was attributed to strong precipitation (Pan et al., 2010; Steffen and Bourassa, 2018). In this study, we found that the barrier layers appeared alternatively may due to synchronous heavy precipitation and strong mixing (Figs 7c–f). In addition, it can be seen that the barrier layer formed on September 24 (Figs 6q–t)

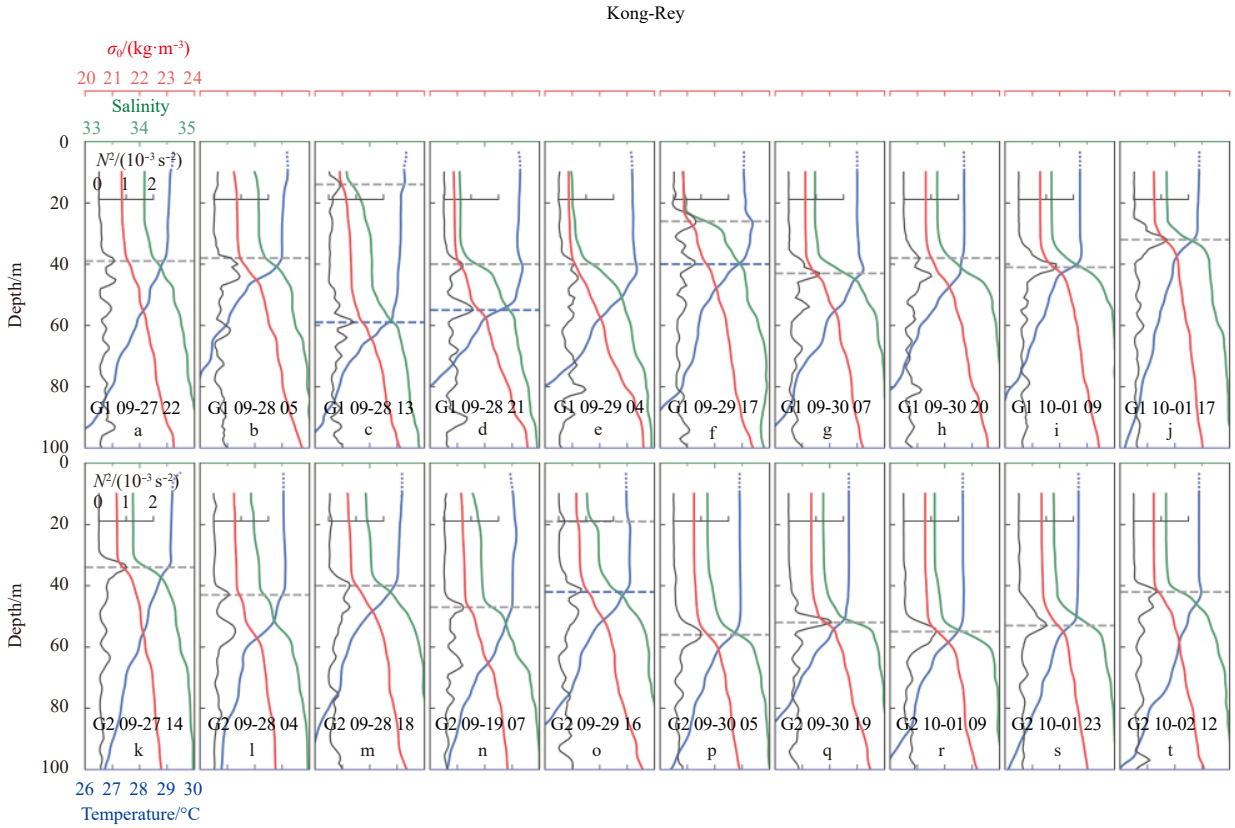

Fig. 7. Sequences of thermohalinic profiles during TC Kong-Rey. Texts inside frame identify the gliders (G1 for Glider 1, G2 for Glider 2), dates and hours. Horizontal dotted lines indicate the MLD (in grey) or ILD (in blue, in case not equal to MLD).

after a relative heavy precipitation on September 22 and 23 could be caused by another formation mechanism, the advection mechanism of barrier layer formation, which was rarely reported by previous studies. most of the barrier layers were accompanied with temperature inversions which may be related to different physical mechanisms. Figures 7d and f shows that the temperature inversion reached about 0.3°C during TC Kong-Rey at the barrier layer. The reason can be explained as the solar radiation could penetrate both of the mixed layer and the barrier layer while heat loss caused by non-solar heat-budget was only confined in the mixed layer, resulting in heat accumulation and temperature rise in the barrier layer (Cronin and McPhaden, 2002; Pan et al., 2010). Relatively small temperature inversion of <0.2°C was developed in the barrier layer during TC Trami (Figs 6r–t), likely attributable to the advection of lower temperature water mass that reduced temperature at the mixed layer and formed the temperature inversion.

4.4 *Spatial variation of thermohaline structure*

Generally, thermohaline structure varies spatially due to the inhomogeneity of temperature and salinity in oceans. Our results suggested that this kind of variation was significant in a small even in this small region during TC period. Figures 7i and r shows that the difference of the MLD reached about 6.0 m between the two glider profiles with 23 km distance at the same moment during TC Kong-Rey. the difference of barrier layer reached about 9.0 m between two glider profiles with 70 km distance (Figs 7f and o). Even more, the difference of the MLD was augmented to 12.0 m between the two glider profiles with 70 km distance at the same moment during TC Trami (Figs 6g and o). a barrier layer with 18.0 m thickness was observed by the Glider 1, but no barrier layer was found by the Glider 2. These results indicated that unignorable bias exists in thermohalinic structure of the upper ocean within a distance <100 km. However, most studies applied drifting Argo float profiles with ⩾100 km distance to identify thermohaline structure response to TC (Park et al., 2011; Wang et al., 2016; Steffen and Bourassa, 2018). In addition, drifting Argo float sampled a profile with 5–7 d usually. This is insufficient to diagnose high-frequency variation of thermohaline structure in spatial and temporal during TC. To achieve that, the advanced remote-controllable glider should be encouraged to use for the purpose in the future.

5 Summary

In this study, we investigated the upper ocean response to three TCs (namely Mangkhut, Trami and Kong-Rey) over the Northwestern Pacific during fall 2018 by underwater glider *in-situ* observation and reanalysis dataset from ERA5. Results showed that the three TC-induced SST cooling were about 0.7°C, 0.5°C, and 0.7°C with different distances to the TC tracks of 315 km, 455 km and 172 km respectively. satellite-derived SST did not show such strong cooling to TCs in the observed region, which might be due to missing observations under severe weather conditions. Modulated by TCs, the mixed layers were deepened in different levels under different cases. Our gliders observed high-frequency variations of MLD and the stratification destruction and construction processes in the upper ocean during TCs. This high-frequency varied thermohaline structure might be related to solar radiation, tide and inertial oscillations. Barrier layers accompanied with temperature inversions showed up in the ob-

served area during TC Trami and TC Kong-Rey due to the TC-induced heavy rainfalls. the thickness of barrier layer can reach about 45 m in some cases. The varying intensities of temperature inversion under different TCs conditions suggested diversity in its driving mechanisms.

Acknowledgements

We thank the crew of R/V *Tansuoyihao* survey vessel from the IDSSE for helping data collection.

References

Balaguru K, Chang P, Saravanan R, et al. 2012. The barrier layer of the Atlantic warmpool: formation mechanism and influence on the mean climate. Tellus A: Dynamic Meteorology and Oceanography, 64(1): 18162, doi: 10.3402/tellusa.v64i0.18162

Bender M A, Ginis I, Kurihara Y. 1993. Numerical simulations of tropical cyclone-ocean interaction with a high-resolution coupled model. Journal of Geophysical Research: Atmospheres, 98(D12): 23245–23263, doi: 10.1029/93JD02370

Bhaskar T V S U, Rahman S H, Pavan I D, et al. 2009. Comparison of AMSR-E and TMI sea surface temperature with Argo near-surface temperature over the Indian Ocean. International Journal of Remote Sensing, 30(10): 2669–2684, doi: 10.1080/01431160802555796

Carvalho F, Kohut J, Oliver M J, et al. 2017. Defining the ecologically relevant mixed-layer depth for Antarctica's coastal seas. Geophysical Research Letters, 44(1): 338–345, doi: 10.1002/2016GL071205

Cione J J, Uhlhorn E W. 2003. Sea surface temperature variability in hurricanes: Implications with respect to intensity change. Monthly Weather Review, 131(8): 1783–1496, doi: 10.1175//2562.1

Cronin M F, McPhaden M J. 2002. Barrier layer formation during westerly wind bursts. Journal of Geophysical Research: Oceans, 107(C12): SRF 21-1–SRF 21-12, doi: 10.1029/2001JC001171

Dare R A, McBride J L. 2011. Sea surface temperature response to tropical cyclones. Monthly Weather Review, 139(12): 3798–3808, doi: 10.1175/MWR-D-10-05019.1

D'Asaro E A, Sanford T B, Niiler P P, et al. 2007. Cold wake of hurricane Frances. Geophysical Research Letters, 34(15): L15609, doi: 10.1029/2007GL030160

Domingues R, Goni G, Bringas F, et al. 2015. Upper ocean response to Hurricane Gonzalo (2014): Salinity effects revealed by targeted and sustained underwater glider observations. Geophysical Research Letters, 42(17): 7131–7138, doi: 10.1002/2015GL065378

Elsner J B, Liu K B. 2003. Examining the ENSO-typhoon hypothesis. Climate Research, 25(1): 43–54

Emanuel K. 2001. Contribution of tropical cyclones to meridional heat transport by the oceans. Journal of Geophysical Research: Atmospheres, 106(D14): 14771–14781, doi: 10.1029/2000JD900641

Emanuel K. 2003. Tropical cyclones. Annual Review of Earth and Planetary Sciences, 31: 75–104, doi: 10.1146/annurev.earth.31.100901.141259

Emanuel K A. 1986. An air-sea interaction theory for tropical cyclones. Part I: Steady-state maintenance. Journal of the Atmospheric Sciences, 43(6): 585–605, doi: 10.1175/1520-0469(1986)043<0585:AASITF>2.0.CO;2

Ginis I. 2002. Tropical cyclone-ocean interactions. Advances in Fluid Mechanics, 33: 83–114

Guo Yipeng, Tan Zhemin. 2018. Westward migration of tropical cyclone rapid-intensification over the Northwestern Pacific during short duration El Niño. Nature Communications, 9(1): 1507, doi: 10.1038/s41467-018-03945-y

Hart R E. 2011. An inverse relationship between aggregate northern hemisphere tropical cyclone activity and subsequent winter climate. Geophysical Research Letters, 38(1): L01705, doi: 10.1029/2010GL045612

Holte J, Talley L. 2009. A new algorithm for finding mixed layer depths with applications to Argo data and Subantarctic Mode Water formation. Journal of Atmospheric and Oceanic Technology, 26(9): 1920–1939, doi: 10.1175/2009JTECHO543.1

Huang Peisheng, Sanford T B, Imberger J. 2009. Heat and turbulent kinetic energy budgets for surface layer cooling induced by the passage of Hurricane Frances (2004). Journal of Geophysical Research: Oceans, 114(C12): C12023, doi: 10.1029/2009JC005603

Jourdain N C, Lengaigne M, Vialard J, et al. 2013. Observation-based estimates of surface cooling inhibition by heavy rainfall under tropical cyclones. Journal of Physical Oceanography, 43(1): 205–221, doi: 10.1175/JPO-D-12-085.1

Kim E J, Kang S K, Jang S T, et al. 2010. Satellite-derived SST validation based on *in-situ* data during summer in the East China Sea and western North Pacific. Ocean Science Journal, 45(3): 159–170, doi: 10.1007/s12601-010-0014-3

Lin I, Liu W T, Wu C C, et al. 2003. New evidence for enhanced ocean primary production triggered by tropical cyclone. Geophysical Research Letters, 30(13): 1718, doi: 10.1029/2003GL017141

Liu Zenghong, Xu Jianping, Sun Chaohui, et al. 2014. An upper ocean response to Typhoon Bolaven analyzed with Argo profiling floats. Acta Oceanologica Sinica, 33(11): 90–101, doi: 10.1007/s13131-014-0558-7

Liu Zenghong, Xu Jianping, Zhu Bokang, et al. 2007. The upper ocean response to tropical cyclones in the northwestern Pacific analyzed with Argo data. Chinese Journal of Oceanology and Limnology, 25(2): 123–131, doi: 10.1007/s00343-007-0123-8

Mei W, Lien C C, Lin I I, et al. 2015. Tropical cyclone-induced ocean response: A comparative study of the South China Sea and tropical northwest Pacific. Journal of Climate, 28(15): 5952–5968, doi: 10.1175/JCLI-D-14-00651.1

Meyers P C, Shay L K, Brewster J K, et al. 2016. Observed ocean thermal response to Hurricanes Gustav and Ike. Journal of Geophysical Research: Oceans, 121(1): 162–179, doi: 10.1002/2015JC010912

Pan Aijun, Wan Xiaofang, Chen Hangyu, et al. 2010. Diurnal evolution of the barrier layer and its local feedback in the central Taiwan Strait. Science China Earth Sciences, 53(2): 274–283, doi: 10.1007/s11430-009-0102-3

Pan Jiayi, Sun Yujuan. 2013. Estimate of ocean mixed layer deepening after a typhoon passage over the South China Sea by using satellite data. Journal of Physical Oceanography, 43(3): 498–506, doi: 10.1175/JPO-D-12-01.1

Park J J, Kwon Y O, Price J F. 2011. Argo array observation of ocean heat content changes induced by tropical cyclones in the North Pacific. Journal of Geophysical Research: Oceans, 116(C12): C12025, doi: 10.1029/2011JC007165

Peng Shiqiu, Zhu Yuhang, Li Zhijin, et al. 2019. Improving the real-time marine forecasting of the northern South China Sea by assimilation of glider-observed T/S profiles. Scientific Reports, 9: 17845, doi: 10.1038/s41598-019-54241-8

Price J F. 1981. Upper ocean response to a hurricane. Journal of Physical Oceanography, 11(2): 153–175, doi: 10.1175/1520-0485(1981)011<0153:UORTAH>2.0.CO;2

Qiu Chunhua, Huo Dan, Liu Changjian, et al. 2019a. Upper vertical structures and mixed layer depth in the shelf of the northern South China Sea. Continental Shelf Research, 174: 26–34, doi: 10.1016/j.csr.2019.01.004

Qiu Chunhua, Mao Huabin, Liu Hailong, et al. 2019b. Deformation of a warm eddy in the northern South China Sea. Journal of Geophysical Research: Oceans, 124(8): 5551–5564, doi: 10.1029/2019JC015288

Qiu Chunhua, Mao Huabin, Wang Yanhui, et al. 2019c. An irregularly shaped warm eddy observed by Chinese underwater gliders. Journal of Oceanography, 75(2): 139–148, doi: 10.1007/s10872-018-0490-0

Qiu Chunhua, Mao Huabin, Yu Jiancheng, et al. 2015. Sea surface cooling in the Northern South China Sea observed using Chinese sea-wing underwater glider measurements. Deep Sea Research Part I: Oceanographic Research Papers, 105: 111–118, doi: 10.1016/j.dsr.2015.08.009

Shu Yeqiang, Xiu Peng, Xue Huijie, et al. 2016. Glider-observed anticyclonic eddy in northern South China Sea. Aquatic Ecosystem

Health & Management, 19(3): 233–241
Sprintall J, Tomczak M. 1992. Evidence of the barrier layer in the surface layer of the tropics. Journal of Geophysical Research: Oceans, 97(C5): 7305–7316, doi: 10.1029/92JC00407
Sriver R L, Huber M. 2007. Observational evidence for an ocean heat pump induced by tropical cyclones. Nature, 447(7144): 577–580, doi: 10.1038/nature05785
Steffen J, Bourassa M. 2018. Barrier layer development local to tropical cyclones based on argo float observations. Journal of Physical Oceanography, 48(9): 1951–1968, doi: 10.1175/JPO-D-17-0262.1
Sutherland G, Reverdin G, Marié L, et al. 2014. Mixed and mixing layer depths in the ocean surface boundary layer under conditions of diurnal stratification. Geophysical Research Letters, 41(23): 8469–8476, doi: 10.1002/2014GL061939
Thomson R E, Fine I V. 2003. Estimating mixed layer depth from oceanic profile data. Journal of Atmospheric and Oceanic Technology, 20(2): 319–329, doi: 10.1175/1520-0426(2003)020<0319:EMLDFO>2.0.CO;2
Vincent E M, Lengaigne M, Madec G, et al. 2012a. Processes setting the characteristics of sea surface cooling induced by tropical cyclones. Journal of Geophysical Research: Oceans, 117(C2): C02020, doi: 10.1029/2011JC007396
Vincent E M, Lengaigne M, Vialard J, et al. 2012b. Assessing the oceanic control on the amplitude of sea surface cooling induced by tropical cyclones. Journal of Geophysical Research: Oceans, 117(C5): C05023, doi: 10.1029/2011JC007705
Walker N D, Leben R R, Balasubramanian S. 2005. Hurricane-forced upwelling and chlorophyll *a* enhancement within cold-core cyclones in the Gulf of Mexico. Geophysical Research Letters, 32(18): L18610, doi: 10.1029/2005GL023716
Wang Xidong, Han Guijun, Qi Yiquan, et al. 2011. Impact of barrier layer on typhoon-induced sea surface cooling. Dynamics of Atmospheres and Oceans, 52(3): 367–385, doi: 10.1016/j.dynatmoce.2011.05.002
Wang Guihua, Wu Lingwei, Johnson N C, et al. 2016. Observed three-dimensional structure of ocean cooling induced by Pacific tropical cyclones. Geophysical Research Letters, 43(14): 7632–7638, doi: 10.1002/2016GL069605
Wu Lingwei, Ling Zheng. 2015. Analysis of sea surface salinity response to typhoon in the Northwest Pacific based on Argo data. Journal of Marine Sciences (in Chinese), 33(3): 1–6
Yang Bing, Hou Yijun, Hu Po, et al. 2015. Shallow ocean response to tropical cyclones observed on the continental shelf of the northwestern South China Sea. Journal of Geophysical Research: Oceans, 120(5): 3817–3836, doi: 10.1002/2015JC010783
Zhang Han, Chen Dake, Zhou Lei, et al. 2016. Upper ocean response to typhoon Kalmaegi (2014). Journal of Geophysical Research: Oceans, 121(8): 6520–6535, doi: 10.1002/2016JC012064
Zhang Zhixiang, Liu Lingling, Wang Fan. 2019. Oceanic barrier layer variation induced by tropical cyclones in the Northwest Pacific. Journal of Oceanology and Limnology, 37(2): 375–384, doi: 10.1007/s00343-019-8008-1
Zhang Han, Wu Renhao, Chen Dake, et al. 2018. Net modulation of upper ocean thermal structure by Typhoon Kalmaegi (2014). Journal of Geophysical Research: Oceans, 123(10): 7154–7171, doi: 10.1029/2018JC014119